PHYSICAL REVIEW B **75**, 220102(R) (2007)

Raman and infrared spectra of multiferroic bismuth ferrite from first principles

P. Hermet,[1] M. Goffinet,[1] J. Kreisel,[2] and Ph. Ghosez[1]
[1]*Physique Théorique des Matériaux, Université de Liège, B-5, 4000 Sart-Tilman, Belgium*
[2]*Laboratoire des Matériaux du Génie Physique (CNRS), MINATEC-INPG, 38016 Grenoble, France*
(Received 7 May 2007; published 29 June 2007)

The entire zone-center phonon spectrum of the $R3c$ ferroelectric antiferromagnetic phase of bismuth ferrite is computed using a first-principles approach based on density functional theory. Two phonon modes exhibiting eigendisplacement vectors that strongly overlap with the atomic distortions taking place at the ferroelectric structural phase transition are identified and give support to a transition with displacive character. Both Raman and infrared reflectivity spectra are also computed, providing benchmark theoretical results for the assignment of experimental spectra.

DOI: 10.1103/PhysRevB.75.220102 PACS number(s): 78.30.−j, 77.80.−e, 77.84.−s

Magnetoelectrics (ME) are, by definition, materials which exhibit a coupling between their magnetic and electric properties.[1,2] Such materials are currently the subject of intensive investigations because they potentially open the way to totally new applications for multistate memories or within the emerging field of spintronics. Among compounds that are intrinsically ME, *multiferroics* which combine ferromagnetic (or another kind of magnetic order) and ferroelectric (FE) orderings are considered as a very important class of materials,[1] particularly attractive for thin-film applications.[3]

Bismuth ferrite ($BiFeO_3$) is a paradigmatic multiferroic and currently the most studied single-phase ME. The broad interest in this compound can be attributed to some of its intrinsic properties (large polarization, high Curie temperature), but also to its simple distorted perovskite structure, well suited for the combination of experimental and theoretical studies and well adapted for epitaxial growth on a perovskite substrate. Many recent works have considered thin-film configurations.[3,4]

It is worth realizing that, in spite of such an intensive research activity, very little is known about the *basic* properties of $BiFeO_3$, even at the bulk level. The exact amplitude of its spontaneous polarization was the subject of recent debates.[5] The mechanism of its FE phase transition is not yet clearly understood.[6] Relatively little experimental information concerning its dynamical properties is available: Raman and infrared (IR) spectra were measured recently on bulk,[6–8] thin films,[9–11] and ceramics,[12] but these spectra do not always agree and mode assignments remain difficult due to the lack of relevant theoretical support.

In this paper, we investigate the zone-center phonon modes in the FE antiferromagnetic (AFM) $R3c$ phase of $BiFeO_3$ using density functional theory (DFT). We identify two phonon modes that strongly overlap with the atomic distortions taking place at the FE structural phase transition, giving support to a displacive character of this transition. We also report theoretical Raman and IR reflectivity spectra, providing benchmark theoretical data directly useful for the assignments of experimental spectra and clarifying the previously proposed assignments.

DFT calculations were performed within the local spin density approximation (LSDA) as implemented in the ABINIT package.[13] We used plane waves and optimized pseudopotentials.[14] Bismuth $5d$, $6s$, and $6p$ electrons, iron $3s$, $3p$, $3d$, and $4s$ electrons, and oxygen $2s$ and $2p$ electrons were considered as valence states. Convergence was reached for a 50-hartree plane-wave kinetic energy cutoff and a $6\times6\times6$ mesh of special k points. Phonon frequencies, IR reflectivity, and Raman intensities were obtained as described in Refs. 15 and 16. Dynamical matrix, Born effective charge tensors (Z^*), and linear optical susceptibility were computed within a variational approach to density functional perturbation theory.[15] Derivatives of the linear optical susceptibility with respect to atomic displacements were calculated from finite differences.

From the crystallographic point of view, the FE phase of $BiFeO_3$ (stable below $T_c\approx1100$ K) has a ten-atom rhombohedral unit cell that belongs to the space group $R3c$.[17] This structure is usually described as arising from a distortion of a reference $Pm\bar{3}m$ cubic perovskite structure, also considered as the most probable paraelectric state.[6] Linking the $Pm\bar{3}m$ phase to the $R3c$ phase requires combining two independent atomic distortions: (i) an antiferrodistortive motion of the oxygens, η_{AFD}, responsible for the unit cell doubling and that alone would bring the cubic system into an intermediate paraelectric phase of $R\bar{3}c$ symmetry and (ii) a polar distortion, η_{FE}, along the pseudocubic [111] direction that alone would lead to a phase of $R3m$ symmetry.

From the magnetic point of view, $BiFeO_3$ is classified as a G-type antiferromagnet below $T_N\approx640$ K.[17] Superimposed on a perfect AFM ordering, there is in fact at the bulk level a spiral spin structure in which the AFM axis rotates through the crystal with an incommensurate wavelength period of 620 Å.[18] However, as in previous DFT studies,[5,19] this additional feature was neglected in our calculations.

Structural relaxations of the FE-AFM $R3c$ phase and of a hypothetical paraelectric-AFM $R\bar{3}c$ phase were performed until the maximum residual forces (stresses) were less than 8×10^{-6} hartree/bohr (3×10^{-5} hartree/bohr^3). The relaxed parameters and magnetic moment on iron atoms are $a=5.50$ Å, $\alpha=60.13°$, $x_{Fe}=0.231$, $x_O=0.541$, $y_O=0.946$, $z_O=0.399$, and $\mu_{Fe}=3.65\mu_B$ for the $R3c$ phase and $a=5.38$ Å, $\alpha=61.85°$, $x=0.671$, and $\mu_{Fe}=3.70\mu_B$ for the $R\bar{3}c$ phase, in close agreement with previous LSDA calculations[5] and experimental data.[17] From the reduced atomic positions in

TABLE I. Frequencies (cm^{-1}) and assignment of the TO and LO modes of $BiFeO_3$. Experimental IR and Raman (Ra) data concern a ceramic (20 K) (Ref. 12) and a monocrystal (4 K) (Ref. 8), respectively.

TO modes	Calc.	IR	Ra	LO modes	Calc.	IR	Ra
E(TO1)	102	75	77	E(LO1)	104	81	
		96				103	
E(TO2)	152	132	136			143	147
		145		E(LO2)	175	153	
A_1(TO1)	167	167		A_1(LO1)	180	176	176
		228		E(LO3)	237	230	
E(TO3)	237	240				243	
E(TO4)	263	264	265	E(LO4)	264	272	
A_1(TO2)	266			A_1(LO2)	277	292	227
E(TO5)	274	288	279	E(LO5)	332	344	
A_1(TO3)	318	304		E(LO6)	377	367	
E(TO6)	335	347	351	E(LO7)	386	400	
E(TO7)	378	369	375				
		400		A_1(LO3)	428	430	
E(TO8)	409	437	437	E(LO8)	436	467	
		471	473	A_1(LO4)	535	501	490
E(TO9)	509	523	525	E(LO9)	547	546	
A_1(TO4)	517	557				601	

these two phases, we deduced η_{AFD} and η_{FE} atomic distortions. The following phonon calculations have been performed in the theoretically optimized FE-AFM $R3c$ phase, considering Cartesian coordinates with the z axis aligned along the polar axis of $BiFeO_3$ ([111] pseudocubic direction).

The zone-center optical phonon modes of the $R3c$ phase can be classified, according to its irreducible representations, into $4A_1 \oplus 5A_2 \oplus 9E$. The A_1 modes polarized along z and the doubly degenerate E modes polarized in the x-y plane are both Raman and IR active while the A_2 modes are silent. The computed frequencies of the A_2 modes are, respectively, 109, 261, 308, 446, and 579 cm^{-1}. These frequencies, however, cannot be compared to experimental values since no experimental inelastic neutron scattering data are presently available.

Table I summarizes the computed frequencies of the transverse (TO) and longitudinal (LO) optic modes of A_1 and E symmetry. Bi atoms only participate in low-frequency modes up to 167 cm^{-1} while oxygen motion strongly dominates in modes above 262 cm^{-1}. Fe atoms are mainly involved in modes between 152 and 261 cm^{-1} but also contribute to some higher-frequency modes. Contrary to what was assumed by Singh *et al.*,[9,10] we notice that the LO-TO splitting is not negligible for all modes in $BiFeO_3$ and can be as large as 100 cm^{-1}.

Interestingly, inspection of the phonon eigendisplacement vectors[24] allows one to point out that the A_1(TO1) mode at 167 cm^{-1} has an overlap of 0.85 with the distortion pattern η_{FE} while the A_1(TO2) mode at 266 cm^{-1} has an overlap of 0.93 with η_{AFD}. The complete overlap matrix is summarized in Table II. The survival into the FE phase of a low-frequency TO mode that strongly overlaps with the FE distortion was previously highlighted in the $R3c$ phase of $LiNbO_3$.[20] It gives strong support to a displacive phase transition mechanism from the $Pm\bar{3}m$ to $R3c$ phase, with a possible intermediate phase of $R\bar{3}c$ or $R3m$ symmetry depending on which instability freezes in first. Moreover, our calculations indicate which modes should *a priori* exhibit the strongest anomaly around T_c.

TABLE II. Overlap (Ref. 24) between the eigendisplacement vectors of A_1(TO) modes of the $R3c$ phase of $BiFeO_3$ and the atomic distortions η_{FE} and η_{AFD}.

Modes	A_1(TO1)	A_1(TO2)	A_1(TO3)	A_1(TO4)
η_{FE}	0.85	0.17	0.49	0.10
η_{AFD}	0.13	0.93	0.34	0.08

Panels (A) and (B) of Fig. 1 display the calculated IR reflectivity spectra (without damping) at normal incidence, respectively, on the [001] and [100] surfaces of a $BiFeO_3$ monocrystal. Moreover, since the only presently available experimental IR data concern a ceramic,[12] we report in panel (C) the corresponding average reflectivity spectrum, assuming a quasicontinuous and random distribution of crystallite orientations.[21] An overall good agreement between theory and experiment is observed both for frequency positions and peak intensities, although the lowest and highest modes present systematic upshifts and downshifts in frequency, respectively. This can be at least partly attributed to the strong anharmonicity of these modes, experimentally evidenced by their temperature dependence.[12] In spite of the similar shape of calculated and experimental IR reflectivity spectra, we notice that the assignment of the experimental modes, further discussed below, remains difficult because 17 TO modes are obtained by Kamba *et al.*[12] from the fit of the experimental

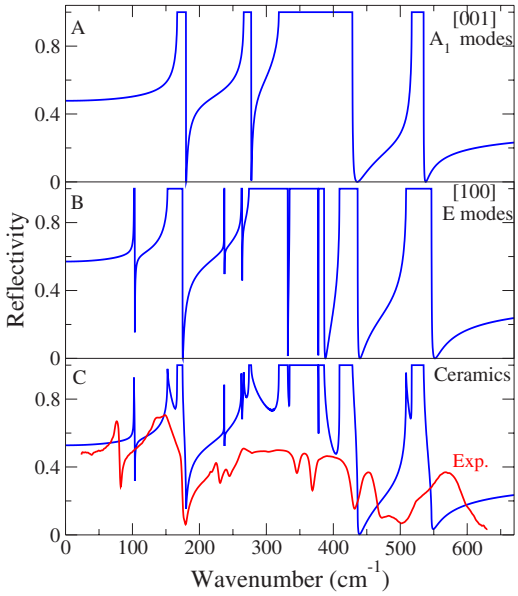

FIG. 1. (Color online) Calculated IR reflectivity spectra (blue) of a $BiFeO_3$ monocrystal (A), (B) and ceramics (C). Experimental data (20 K) from Ref. 12 (red).

TABLE III. Theoretical main values of the IR oscillator strength tensor $\tilde{S}$ ($\times 10^{-5}$a.u.) and Raman intensities ($\times 10^{-5}$ bohr^3) of the TO modes in a $BiFeO_3$ monocrystal.

	Infrared			Raman	
Modes	$S_{xx}=S_{yy}$	S_{zz}	Powder	$a^2(c^2)$	$b^2(d^2)$
E(TO1)	2.43	0	1.62	(1.52)	(0.68)
E(TO2)	45.48	0	30.32	(4.84)	(1.04)
A_1(TO1)	0	19.15	6.38	5.03	1.81
E(TO3)	1.24	0	0.83	(0.02)	(31.09)
E(TO4)	19.16	0	12.77	(7.04)	(2.62)
A_1(TO2)	0	35.55	11.85	0.00	1.86
E(TO5)	156.46	0	104.31	(1.60)	(103.41)
A_1(TO3)	0	110.43	36.81	2.12	161.39
E(TO6)	5.62	0	3.75	(2.58)	(12.62)
E(TO7)	0.26	0	0.17	(39.37)	(1.95)
E(TO8)	12.56	0	8.37	(0.17)	(6.24)
E(TO9)	34.03	0	22.69	(27.12)	(3.76)
A_1(TO4)	0	14.46	4.82	5.97	109.87

spectrum (see Table I) while only 13 TO modes are theoretically permitted. Computed IR oscillator strengths of the A_1(TO) and E(TO) modes are reported in Table III and might be valuable for the interpretation of IR transmission spectra. We observe that the A_1(TO1) mode, related to the FE distortion η_{FE}, is not the mode with the highest polarity as often observed in typical FE.[20] Also, the A_1(TO2) mode has a quite large oscillator strength. This is surprising in view of its strong overlap with η_{AFD} (a nonpolar AFD oxygen motion in the $Pm\bar{3}m$ reference phase) but it is made possible by both the decrease of symmetry of the Z^* in the $R3c$ phase and additional other polar contributions to A_1(TO2).

Within the previously defined system of coordinates, the Raman susceptibility tensors of A_1 and E modes can be written as

$$A_1(z)=\begin{pmatrix} a & \cdot & \cdot \\ \cdot & a & \cdot \\ \cdot & \cdot & b \end{pmatrix}, \quad E(x)=\begin{pmatrix} c & \cdot & d \\ \cdot & -c & \cdot \\ d & \cdot & \cdot \end{pmatrix},$$

$$E(y)=\begin{pmatrix} \cdot & -c & \cdot \\ -c & \cdot & d \\ \cdot & d & \cdot \end{pmatrix}.$$

Theoretical absolute values of the Raman coefficients are reported in Table III. Figures 2(a) and 2(b) display the calculated Raman spectra of a $BiFeO_3$ monocrystal in the $x(zz)y$ and $z(xy)\bar{z}$ configurations for which, in principle, only pure A_1(TO) and E(TO) modes can respectively be detected. The Raman line shape is assumed to be Lorentzian, and the linewidth is fixed at 4 cm^{-1}. Configurations like $x(zz)y$ restricted to pure A_1(TO) modes might be considered as the most appropriate to follow the potential soft-mode behavior of A_1(TO1) and A_1(TO2) modes around T_c. Unfortunately, the

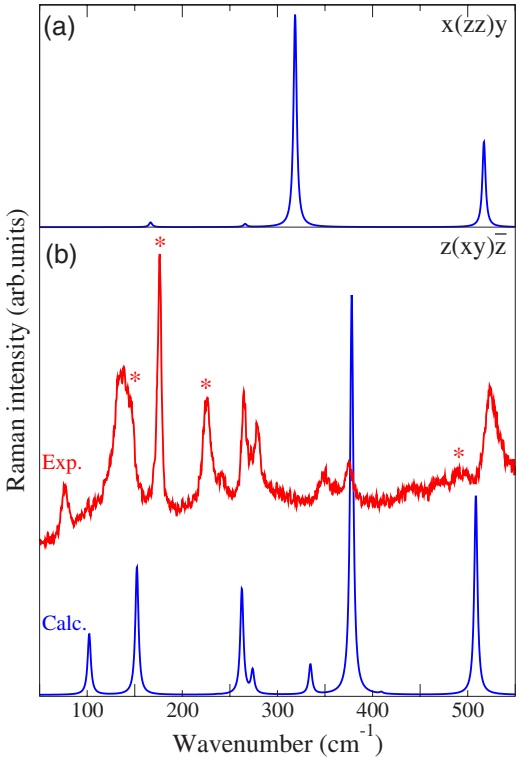

FIG. 2. (Color online) Calculated (blue) Raman spectrum of $BiFeO_3$ in comparison to experimental (red) data at 4 K (Ref. 8). Asterisks in the experimental spectrum locate A_1 modes which do not completely disappear in crossed polarization.

modes of interest have weak intensities in those configurations, suggesting that IR measurements might be preferred instead for the purpose of identifying a potential softening of A_1 modes. Interpretation of the experimental Raman spectra of $BiFeO_3$ is presently subject to controversy. Measurements on monocrystal with parallel $z(xx)\bar{z}$ configuration [yielding lines for both E(TO) and A_1(LO) modes] and crossed $z(xy)\bar{z}$ configuration [yielding lines for E(TO) modes only] reported independently by Haumont *et al.*[7] and by Fukumura *et al.*[8] differ significantly. In Fig. 2, good agreement is observed between our calculations and the experimental spectrum of Fukumura *et al.* for both frequency positions and relative intensities. Our theoretical data are also compatible with the measurements on film by Singh *et al.*[10] Unfortunately, such an agreement cannot be achieved with the results of Haumont *et al.*,[7] suggesting the presence of additional effects in their case and asking for better characterization of their sample. For instance, stoichiometry problems can potentially affect the spectrum, as previously reported for $LiNbO_3$.[22]

Our calculations can now be used to propose a coherent assignment of experimental Raman and IR spectra as detailed in Table I. We notice that direct measurements on monocrystal have only been reported for A_1(LO) and E(TO) modes,[8] which will be discussed in further detail below, while the positions of A_1(TO) and E(LO) were only estimated from a fit of IR reflectivity on ceramics.[12]

First, concerning the E(TO) modes, IR and Raman data are in agreement with our calculations (frequencies and intensities) for the eight experimental modes centered around

76, 134, 264, 283, 349, 372, 437, and 524 cm^{-1}. For the last mode, analysis of the experimental Raman spectrum suggests a frequency at 473 cm^{-1}, in agreement with an IR peak at 471 cm^{-1}, while the calculation predicts an E(TO3) mode at 237 cm^{-1} in agreement with another IR peak measured at 240 cm^{-1}. Further inspection of the experimental Raman spectra supports the E symmetry assignment to the line at 240 cm^{-1} with a weak intensity in agreement with our calculation, rather than at 473 cm^{-1} because (i) a weak line centered at 240 cm^{-1} is clearly observed in the experimental Raman spectrum for crossed polarization and is still likely present for parallel polarization, although hidden in the foot of the line at 227 cm^{-1}, and (ii) the mode at 473 cm^{-1} measured for parallel polarization completely disappears for crossed polarization, suggesting that it is rather an A_1 mode than an E mode. This assignment is also supported by the Raman detection of an A_1 mode at 425 cm^{-1} in films.[10]

Concerning now the A_1(LO) modes, the theoretical prediction might be less accurate than for TO modes due to typical LDA inaccuracy in the prediction of the LO-TO splitting[23] so that the assignment is less obvious. Fukumura *et al.*[8] report four frequencies at 147, 176, 227, and 490 cm^{-1} while our previous discussion suggests an additional A_1 mode at 473 cm^{-1}. The modes at 176 and 490 cm^{-1} can be unambiguously associated with theoretical frequencies at 180 and 535 cm^{-1}. Theoretical frequencies at 277 and 428 cm^{-1} can also be convincingly related to the experimental modes at 227 and 473 cm^{-1}. This assignment therefore leaves the line at 147 cm^{-1} as the only unassigned experimental one. This is surprising since this line neatly appears and is reported in Raman for bulk and thin films, and also in IR. However, an error in the theoretical prediction is relatively unlikely in view of the overall good agreement obtained. We checked that working at the experimental volume or using generalized gradient approximation (GGA) or GGA+U functionals does not affect the present discussion. The neglect of spin-orbit coupling for Bi might slightly shift the position of the lowest A_1 mode dominated by Bi motion but not the whole set of A_1 frequencies. It seems also unlikely to have three of the four A_1 modes below 230 cm^{-1} in view of the disparity of masses of the three types of atom. Our calculations therefore directly question the origin of the line at 147 cm^{-1} and request further experimental investigation on monocrystals.

In this Rapid Communication, we have reported first-principles calculations of the IR reflectivity and Raman spectra of $BiFeO_3$, providing valuable information about the lattice dynamics of this compound. It has also allowed a coherent assignment of experimental IR and Raman spectra. We hope that this work will motivate complementary experimental investigations of monocrystals to confirm our assignments and the displacive character of the FE phase transition.

We thank U. V. Waghmare for sharing pseudopotentials and H. Béa, S. Kamba, R. Haumont, and H. Fukumura for sending their experimental data. M.G. is grateful to FNRS-Belgium. Calculations were partly performed at CISM (UCL-Belgium, Project FRFC No. 2.4502.05). This work was supported by the European STREP MaCoMuFi, the VolkswagenStiftung, and the European FAME-NoE.

[1] M. Fiebig, J. Phys. D **38**, R123 (2005).
[2] W. Eerenstein, N. D. Mathur, and J. F. Scott, Nature (London) **442**, 759 (2006).
[3] R. Ramesh and N. A. Spaldin, Nat. Mater. **6**, 21 (2007).
[4] J. Wang *et al.*, Science **299**, 1719 (2003).
[5] J. B. Neaton *et al.*, Phys. Rev. B **71**, 014113 (2005).
[6] R. Haumont *et al.*, Phys. Rev. B **73**, 132101 (2006).
[7] R. Haumont, J. Kreisel, and P. Bouvier, Phase Transitions **79**, 1043 (2006).
[8] H. Fukumura *et al.*, J. Magn. Magn. Mater. **310**, e367 (2007).
[9] M. K. Singh, S. Ryu, and H. M. Jang, Phys. Rev. B **72**, 132101 (2005).
[10] M. K. Singh *et al.*, Appl. Phys. Lett. **88**, 042907 (2006).
[11] H. Béa *et al.*, Philos. Mag. Lett. **87**, 165 (2007).
[12] S. Kamba *et al.*, Phys. Rev. B **75**, 024403 (2007).
[13] X. Gonze *et al.*, Comput. Mater. Sci. **25**, 478 (2002).
[14] A. M. Rappe *et al.*, Phys. Rev. B **41**, 1227 (1990).
[15] X. Gonze and C. Lee, Phys. Rev. B **55**, 10355 (1997).
[16] P. Hermet *et al.*, J. Phys. Chem. B **110**, 24869 (2006).
[17] F. Kubel and H. Schmid, Acta Crystallogr., Sect. B: Struct. Sci. **B46**, 698 (1990).
[18] I. Sosnowska, T. Peterlin-Neumaier, and E. Streichele, J. Phys. C **15**, 4835 (1982).
[19] P. Ravindran *et al.*, Phys. Rev. B **74**, 224412 (2006).
[20] M. Veithen, X. Gonze, and Ph. Ghosez, Phys. Rev. Lett. **93**, 187401 (2004).
[21] T. G. Mayerhöfer, Vib. Spectrosc. **35**, 67 (2004).
[22] A. Ridah *et al.*, J. Phys.: Condens. Matter **9**, 9687 (1997).
[23] The LO-TO splitting depends on ϵ^{∞} typically overestimated within the local density approximation and on Z^* observed to be usually dependent on the used functional.
[24] The eigendisplacement vectors η are related to the dynamical matrix eigenvectors γ by $\eta = M^{-1/2}\gamma$ and are normalized such as $\langle \eta | M | \eta \rangle = 1$ where M is the mass matrix (Ref. 15). The overlap between two normalized vectors η_1 and η_2 is therefore defined as $\langle \eta_1 | M | \eta_2 \rangle$.